SI document

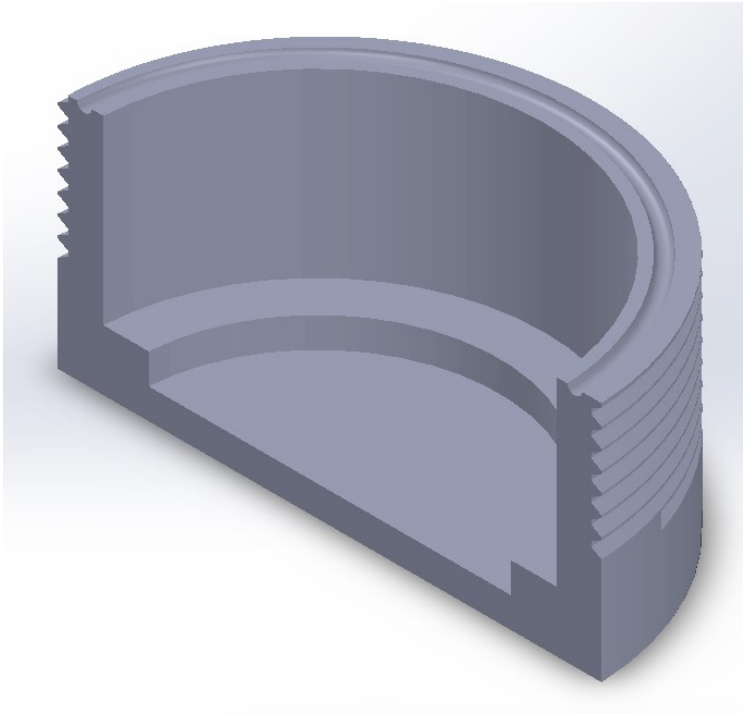

Figure S1- Teflon infiltration chamber body

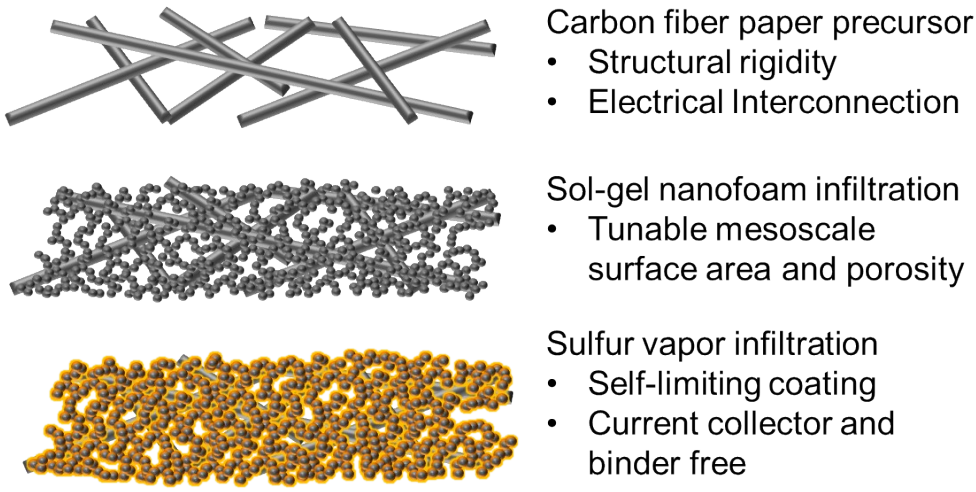

Figure S2. A simplified schematic of the processing of carbon fiber paper into a S@CNFP electrode.

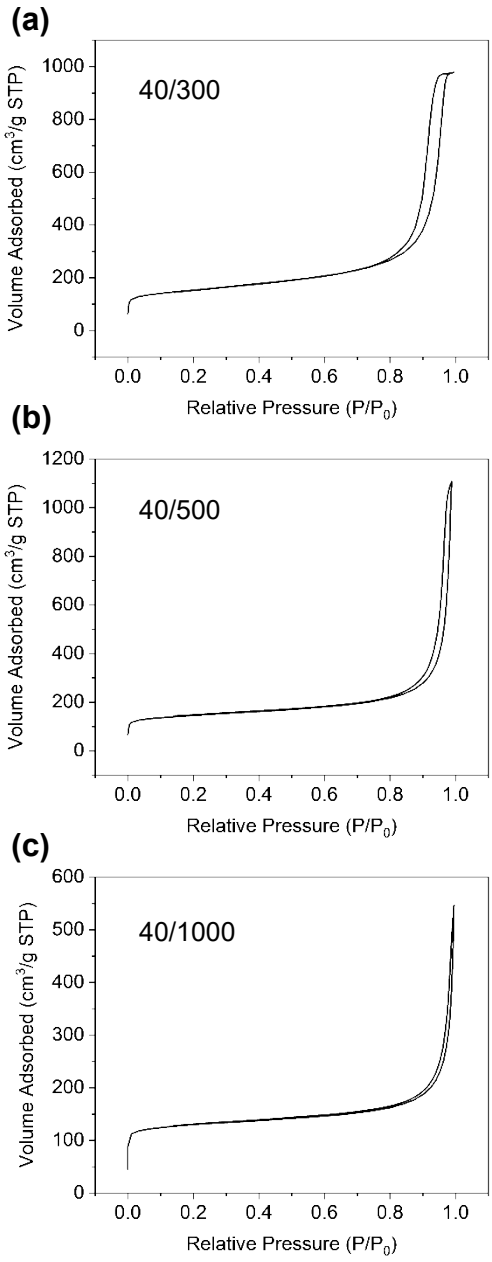

Figure S3. N_2 adsorption isotherms for CNFP-40/300 (a), CNFP-40/500 (b), and CNFP-40/1000 (c).

Table S1. Nominal sulfur coating thicknesses determined using BET surface area and mass loadings.

Infiltration Time (h)	Sulfur Coating Thickness (nm)		
	40/300	40/500	40/1000
2	2.4	1.9	1.1
6	5.3	4.0	1.9
18	8.5	7.3	3.3

Table S2. Occupation of CNFP pores by sulfur for different infiltration durations.

Infiltration Time (h)	Sulfur Pore-volume Occupation (%)		
	40/300	40/500	40/1000
2	13	10	6
6	33	20	9
18	56	37	16

Table S3. Average volumetric sulfur loadings in 1-ply CNFP electrodes.

Infiltration Time (h)	Volumetric Loading ($g_{sulfur}/cm^{-3}_{CNFP}$)		
	40/300	40/500	40/1000
2	0.27	0.21	0.09
6	0.61	0.43	0.16
18	0.98	0.80	0.28

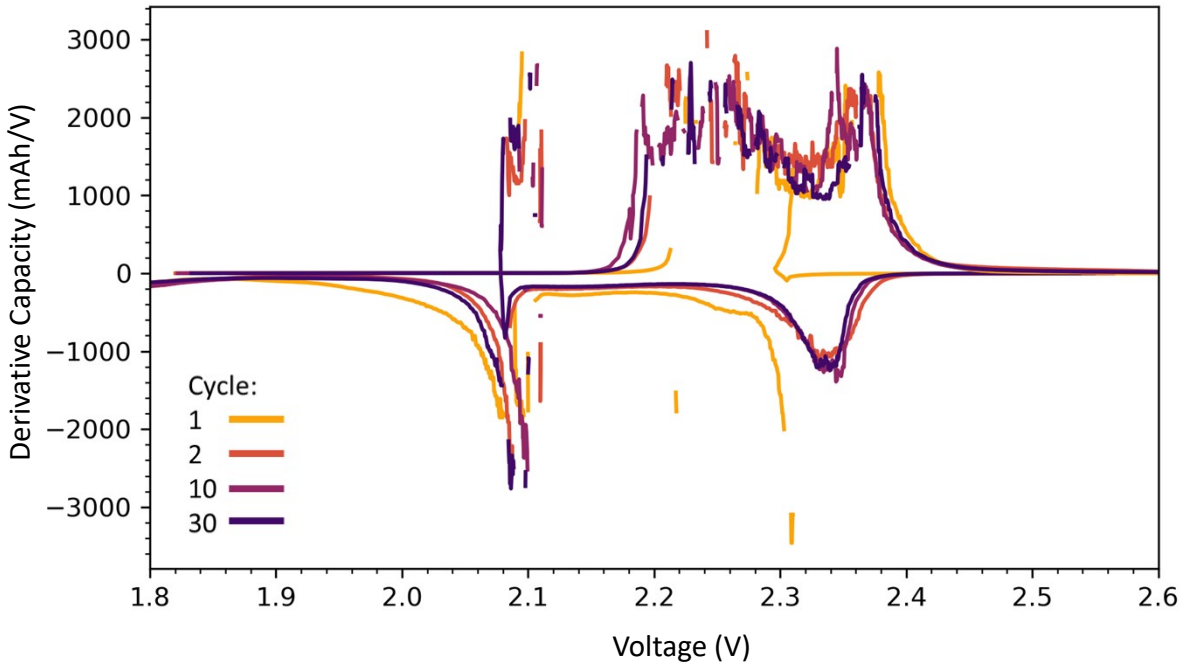

Figure S4- derivative capacity analysis of 40/500- 6hr over cycles 1, 2, 10, and 30

Table S4. Summary of results from Figure 5b varying carbon type and sulfur vapor exposure

Electrode	Sulfur loading (%)	Capacity ($mAh/g_{electrode}$)	Capacity (mAh/g_{sulfur})
S@CNFP-40/1000-2h	17.83	138	1117
S@CNFP-40/1000-6h	27.78	227	787
S@CNFP-40/500-2h	30.79	301	896
S@CNFP-40/300-2h	36.53	300	817
S@CNFP-40/1000-18h	39.75	291	745
S@CNFP-40/500-6h	47.67	350	719
S@CNFP-40/300-6h	56.86	39	67
S@CNFP-40/500-18h	62.58	64	107
S@CNFP-40/300-18h	68.54	8	12

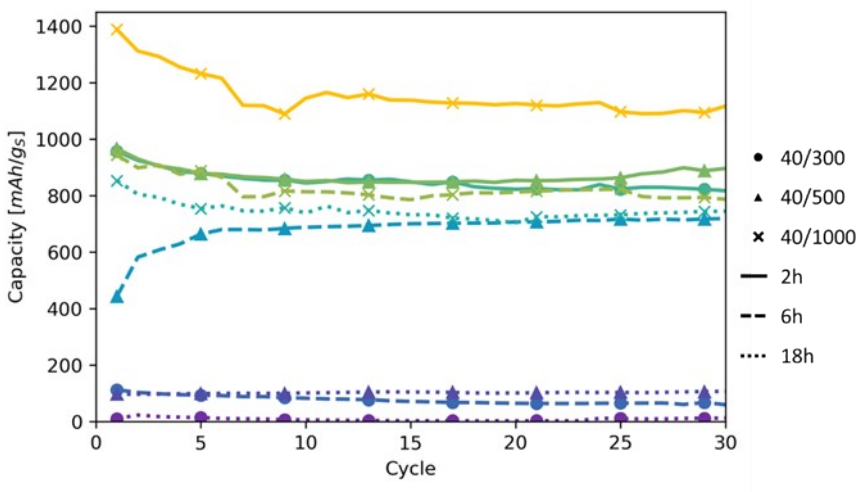

Figure S5. Cycling data of S@CNFP materials normalized to sulfur mass.

This figure shows the inherent bias in the visualization of data. Lower sulfur loadings will characteristically have higher capacity when normalized to the mass of sulfur versus the mass of the entire electrode (i.e. low sulfur loading has highest capacity, mid-range sulfur loading is in the middle, and high sulfur loading has low capacity).

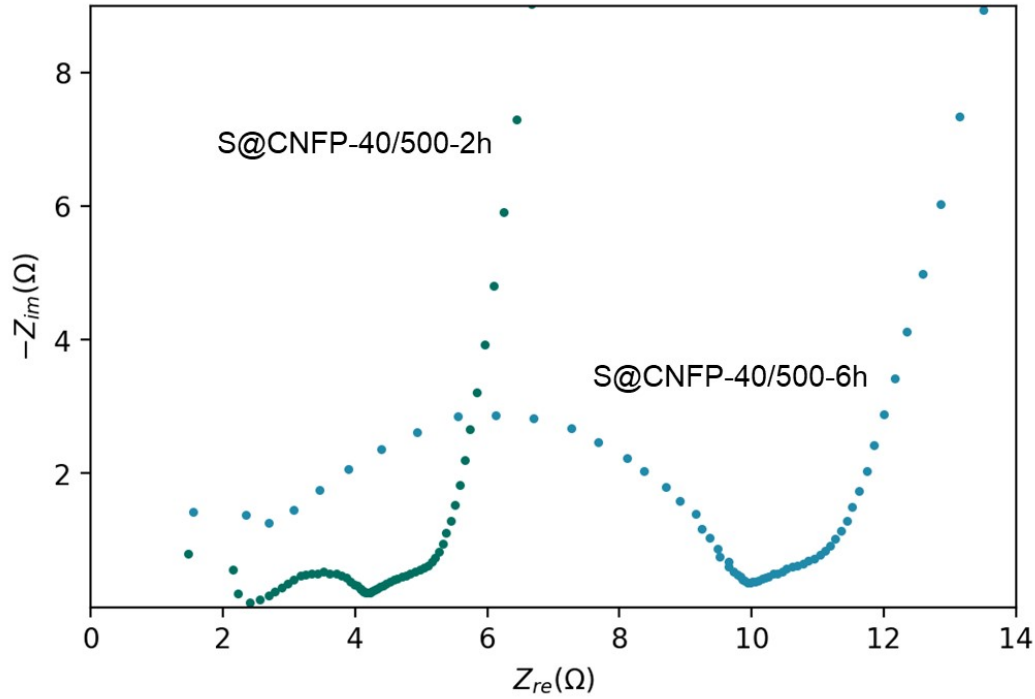

Figure S6- EIS measurements of Li-S full cells fabricated with S@CNFP electrodes of comparable pore structures with different sulfur loadings.

EIS measurements show increased impedance at higher S loadings, indicating higher electrical resistance as the thickness of the sulfur coating of the pores increases.

Table S5. Average mass loadings of sulfur into 40/500 CNFPs of varying (ply count).

Ply	Average sulfur loading (%)	
	2h	6h
1	40	58
2	32	49
3	30	44

Table S6. Comparative sulfur loadings and areal capacities at respective current density. Reference list summarized by Zhou et al.[1]

Electrode Material	Sulfur Loading (mg/cm^2)	Areal Capacity (mAh/cm^2)	Current	Reference
C/S yolk-shell composite	0.5	0.3	3.4 A/g (1.7 mA/cm^2)	[2]
C/S@carbon nanosheet composite	0.7	0.9	1.7 A/g (1.2 mA/cm^2)	[3]
S-infiltrated templated CNTs	0.8	1.2	3.4 A/g (1.7 mA/cm^2)	[4]
C/S composite	0.9	1.3	0.3 A/g (0.3 mA/cm^2)	[5]
Graphene/S composite	1	1	1.7 A/g (1.7 mA/cm^2)	[6]
C/S-PPy composite	2	0.9	0.3 A/g (0.7 mA/cm^2)	[7]
C/S core-shell composite	2	2.2	0.3 A/g (0.7 mA/cm^2)	[8]
C/S composite	4.2	3.3	0.17 A/g (0.7 mA/cm^2)	[9]
Carbon nanofoam	6.4	4.1	0.17 A/g (1.1 mA/cm^2)	This work
ACF cloth	6.5	3.9	0.15 A/g (1.0 mA/cm^2)	[10]
C/c-PANS composite @ Ni coated polyester	6.7	9	0.6 A/g (4.2 mA/cm^2)	[11]
CNT/S composite on Al foam	7	6	0.17 A/g (1.2 mA/cm^2)	[1]
C/S composite on PDMS/graphene foam	10.1	9.3	1.5 A/g (15 mA/cm^2)	[12]
C/S composite on Al foam	18	22	0.017 A/g (0.3 mA/cm^2)	[1]

References

1. G. Zhou, L. Li, C. Ma, S. Wang, Y. Shi, N. Koratkar, W. Ren, F. Li and H.-M. Cheng, *Nano Energy*, 2015, **11**, 356-365.
2. Z. Wei Seh, W. Li, J. J. Cha, G. Zheng, Y. Yang, M. T. McDowell, P.-C. Hsu and Y. Cui, *Nature Communications*, 2013, **4**, 1331.
3. X. a. Chen, Z. Xiao, X. Ning, Z. Liu, Z. Yang, C. Zou, S. Wang, X. Chen, Y. Chen and S. Huang, *Advanced Energy Materials*, 2014, **4**, 1301988.
4. S. Moon, Y. H. Jung, W. K. Jung, D. S. Jung, J. W. Choi and D. K. Kim, *Advanced Materials*, 2013, **25**, 6547-6553.
5. G. Zhou, S. Pei, L. Li, D.-W. Wang, S. Wang, K. Huang, L.-C. Yin, F. Li and H.-M. Cheng, *Advanced Materials*, 2014, **26**, 625-631.
6. M.-Q. Zhao, Q. Zhang, J.-Q. Huang, G.-L. Tian, J.-Q. Nie, H.-J. Peng and F. Wei, *Nature Communications*, 2014, **5**, 3410.
7. Y. Fu and A. Manthiram, *The Journal of Physical Chemistry C*, 2012, **116**, 8910-8915.
8. W. Zhou, Y. Yu, H. Chen, F. J. DiSalvo and H. D. Abruña, *Journal of the American Chemical Society*, 2013, **135**, 16736-16743.

9. J. Song, T. Xu, M. L. Gordin, P. Zhu, D. Lv, Y.-B. Jiang, Y. Chen, Y. Duan and D. Wang, *Advanced Functional Materials*, 2014, **24**, 1243-1250.
10. J.-S. Kim, T. H. Hwang, B. G. Kim, J. Min and J. W. Choi, *Advanced Functional Materials*, 2014, **24**, 5359-5367.
11. X.-B. Cheng, H.-J. Peng, J.-Q. Huang, L. Zhu, S.-H. Yang, Y. Liu, H.-W. Zhang, W. Zhu, F. Wei and Q. Zhang, *Journal of Power Sources*, 2014, **261**, 264-270.
12. H. Nara, T. Yokoshima, H. Mikuriya, S. Tsuda, T. Momma and T. Osaka, *Journal of The Electrochemical Society*, 2017, **164**, A5026.